Geofluids (2007) 7, 441–450 doi: 10.1111/j.1468-8123.2007.00198.x

Modeling CO_2 generation, migration, and titration in sedimentary basins

L. M. CATHLES[1] AND M. SCHOELL[2]

[1]*Department of Earth and Atmospheric Sciences, Cornell University, Ithaca, NY, USA;* [2]*Gas Consult International Inc., Berkeley, CA, USA*

ABSTRACT

High mole fraction CO_2 gases pose a significant risk to hydrocarbon exploration in some areas. The generation and movement of CO_2 are also of scientific interest, particularly because CO_2 is an important greenhouse gas. We have developed a model of CO_2 generation, migration, and titration in basins in which a high mole fraction CO_2 gas is generated by the breakdown of siderite ($FeCO_3$) and magnesite ($MgCO_3$) where parts of the basin are being heated above approximately 330°C. The CO_2 reacts with Fe-, Mg-, and Ca-silicates as it migrates upward and away from the generation zone (CO_2-kitchen). Near the kitchen, where the Fe-, Mg-, and Ca-silicates have been titrated and destroyed by previous packets of migrating CO_2, gas moves upward without lowering its CO_2 mole fraction. Further on, where Fe- and Mg-silicates are still present but Ca-silicates are absent in the sediments, the partial pressure of CO_2 is constrained to 0.1–30 bars and reservoirs contain a few mole percent CO_2 as described by Smith & Ehrenberg (1989). Still further from the source, where Ca-silicates have not been titrated, partial pressure of CO_2 in migrating methane gas are orders of magnitude lower. A 2D numerical model of CO_2 generation, migration, and titration quantifies these buffer relations and makes predictions of CO_2 risk in the South China Sea that are compatible with exploration experience. Reactive CO_2 transport models of the kind described could prove useful in determining how gases migrate in faulted sedimentary basins.

Key words: carbon dioxide, generation, migration, sedimentary basins, titration

Received 23 July 2007; accepted 3 August 2007

Corresponding author: Lawrence M. Cathles, Department of Earth and Atmospheric Sciences, Cornell University, Ithaca, NY 14853-1504, USA.
Email: lmc19@cornell.edu. Tel: 607-255-2844; Fax: 607-254-4780.

Geofluids (2007) 7, 441–450

INTRODUCTION

It has been known for many years that gas reservoirs contain significant mole fractions of CO_2 gas (i.e. Smith & Ehrenberg 1989), with some reservoirs containing >90 wt% CO_2 (e.g. Wycherley *et al.* 1999; Leong 2000). The presence of a few weight percent CO_2 in a reservoir decreases the economic value of the reservoir significantly.

Figure 1 of Hutcheon *et al.* (1993) shows how the partial pressure (fugacity) in bars of CO_2 in reservoirs with intermediate levels of CO_2 (a few up to 10 wt%) depends on temperature, and compares their semi-log linear trend to a similar, but much lower, temperature trend of the CO_2 partial pressures measured in geothermal systems such as those in Iceland. It is immediately apparent from the data in this plot that there is a large difference between P_{CO_2} in igneous hydrothermal systems and P_{CO_2} in gas reservoirs in sedimentary basins. For example, at 100°C the partial pressure of CO_2 in the basin gas reservoirs is 3 orders of magnitude greater than that in the hydrothermal systems in Iceland.

Hutcheon *et al.* (1993) suggested that the different levels of P_{CO_2} might be related to a combination of three factors: (i) the generally very much greater total fluid pressures in sedimentary basins (1000 bars versus <200 bars); (ii) different fluid–rock interaction histories; and (iii) different fluid compositions. Hutcheon *et al.* showed that P_{CO_2} data from hydrothermal areas and sedimentary basins could be simulated by mineral buffers containing margarite with different thermodynamic activity. A margarite activity of 2×10^{-5} simulated observed basin P_{CO_2} versus temperature, whereas a margarite activity of 1.6×10^{-2} simulated

observed hydrothermal P_{CO_2} versus temperature trends. Hutcheon *et al.* offered no explanation of why margarite activity should be different in the two systems. They also computed P_{CO_2} to fit both systems using the geochemical program EQ6 by taking different starting fluid compositions and assuming quartz as a mineral buffer in sedimentary basins and chalcedony in geothermal systems. They used only a partial mineral buffer which lacked any calcium (or iron or magnesium) silicate phase. For this reason, their starting solution composition was a controlling factor on P_{CO_2}. It is not clear why reservoirs that have intermediate levels of CO_2 have a different water chemistry from those much more common reservoirs with negligible levels of CO_2, or from reservoirs with very high levels of CO_2. For example, Hanor (1994) showed that the main controls of brine chemistry in the Gulf of Mexico (and elsewhere) are salinity and temperature. Pore fluid salinity does not correlate with reservoir mole fraction of CO_2.

We argue here that a much better explanation for the variable CO_2 content of gas reservoirs is the one that has been offered by Wilson (1994). He pointed out that field-wide variations in the fugacity of CO_2 are related to differences in the detrital mineral assemblage. Very low CO_2 fugacities (partial pressures in the gas phase) are associated with sediments containing anorthitic plagioclase whereas high CO_2 fugacities are associated with sediments lacking a Ca-aluminosilicate mineral. Wilson states: 'As basinal fluids with an inferred higher f_{CO2} flow into the sandstone, calcite forms at the expense of Ca-bearing silicates while the fluid equilibrates with the minerals. As this continues, ultimately the CO_2-buffer capacity of the sandstone is exceeded when Ca-bearing silicates are gone'. Wilson's suggestion for aluminosilicate titration is the basis for the modeling described here.

Our conceptual model is simple: When temperatures in a basin reach approximately 330°C the partial pressure of CO_2 plus steam exceeds local pore pressure and a separate gas phase is formed. If this CO_2-rich gas steam migrates upward to shallower and cooler environments the steam will condense, and if the CO_2 has not reacted with the rock along the migration pathways, it can fill shallow reservoirs with nearly 100% CO_2 gas and/or vent CO_2 into the atmosphere. If, along the final portion of the path, the Ca-bearing aluminosilicates are titrated, but Fe- or Mg-aluminosilicates are not, the CO_2 partial pressures in the gas phase will lie along the Smith and Ehrenberg trend in Fig. 1. If Ca-aluminosilicate exists along the migration path, the CO_2 partial pressure will be very low and CO_2 will be an insignificant fraction of the reservoir gas.

In a process sense, CO_2 is generated when water reacts with aluminosilicate minerals to produce clays. The H^+ that is left behind when OH^- is used to produce the clay minerals attacks any available carbonates and produces CO_2. If the CO_2 builds up to equilibrium levels the reaction stops after only a little clay is formed and carbonate dissolved. However, if the separation of a CO_2 gas phase keeps the bicarbonate concentration in the pore fluids below saturation, the CO_2-generating reaction will persist until one of the reactants (aluminosilicates or carbonate) is exhausted.

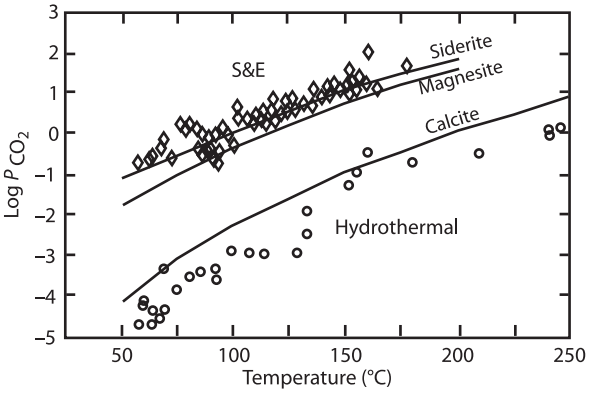

Fig. 1. Symbols show the logarithm (base 10) of the partial pressure of CO_2 (or fugacity of CO_2 indicated by the symbol f_{CO_2}) in bars in sedimentary basins (solid diamonds) and igneous hydrothermal systems (open circles) compiled by Hutcheon *et al.* (1993). The P_{CO_2} values predicted by three mineral buffers (4a–c) are shown by solid lines. The line labeled calcite is calculated from a buffer consisting of calcite, laumontite, kaolinite, and quartz for pressures lying on the two-phase curve of water. The lines labeled 'siderite' and 'magnesite' are calculated for buffers with an Fe- or Mg-silicate but no Ca-silicate. Both these buffer lines are calculated along the basin *P–T* trajectory proposed by Smith & Ehrenberg (1989) in which *P* (bars) = 6 (*T* (°C) − 25). This *P–T* trajectory is shown and compared with others in Fig. 2.

There are many natural and human-induced examples of this kind of CO_2-generating reaction. For example, CO_2 has been produced in copious quantities when 300°C steam was injected at shallow depths to facilitate hydrocarbon recovery. In Chevron's Buena Vista Hills steamflood, the injection of 2.5 million barrels of 300°C steam resulted in the venting of 80 million scf (100 million moles) of CO_2 (Cathles *et al.* 1990). The carbon isotopic signature of the gas produced leaves no doubt that it was derived from carbonate dissolution. The reactions involved in this kind of CO_2 generation have been studied in connection with steam injection into oil sands in Alberta, where it has been found that clay formation invariably accompanies carbonate destruction and CO_2 generation (e.g. Boon & Hitcheon 1983; Kubacki *et al.* 1984; Hebner *et al.* 1986). Laboratory experiments also confirm this relationship (e.g. Levinson & Vian 1966; Baylis & Levinson 1971). Basaltic intrusion in the Salton Sea geothermal area produced a separate CO_2 gas phase when naturally convecting ground waters were heated to approximately 350°C. In this case the CO_2 was trapped in the adjacent Imperial Carbon Dioxide Gas Field. Between 1934 and 1954 over 18.4 million m^3 of CO_2 was produced from this reservoir to make dry ice (Muffler and White 1968).

Two issues must be clarified to understand how CO_2 might be generated and trapped in sedimentary basins: First we must understand where and how in basins a separate CO_2-rich gas phase can be generated. This we do in the following section by (i) considering the rock-buffered concentration of CO_2 dissolved in the pore fluid as a function of temperature, and (ii) determining when and where it could be high enough for a separate CO_2-rich gas phase to be formed. Second, we need to understand what is required for the CO_2 to migrate to shallower reservoirs without being consumed by carbonate-forming reactions. In the section following the next, we describe our numerical approach to this issue.

THE SOURCE OF CO_2 GAS

Above approximately 70°C the pore fluids in sedimentary basins and in igneous geothermal systems are in equilibrium with the host minerals (Ellis 1970; Elder 1981; Giggenbach 1981, 1997; Arnorsson *et al.* 1983; Henley *et al.* 1984; Cathles 1986, 1993; Hanor 2001; Palandri & Reed 2001). This fundamentally important observation means, among other things, that the chemistry of the pore fluids can be computed using the mass action equation as a function of temperature, pressure and salinity, if the set of buffer minerals is specified. The buffer minerals specify the activity ratios (to H^+) of the basis species such as $Ca^{++}/(H^+)^2$, Na+/H^+, K^+/H^+, etc. To obtain the buffered chemistry of the solution, pH is usually determined by charge balance and the solution chemistry then calculated by summing the concentrations of all complexes of the basis species. In the present case, however, the partial pressure of carbon dioxide, P_{CO_2}, which also equals the activity of CO_2 because the activity coefficient of the dissolved CO_2 is 1, can be directly calculated from the bicarbonate activity ratio.

The mass action equation states that the stoichiometric matrix describing the dissolution of the buffer minerals, S_m multiplied by the log activity of the basis species, L_{ab}, equals the log K of the buffer dissolution reactions, L_K:

$$S_m L_{ab} = S'_m L'_{ab} + S_{H+} L_{a_{H+}} + S_{H_2O} L_{a_{H_2O}} = L_K. \qquad (1)$$

In the second expression (right-hand side of the first equal sign), we have taken the H^+ and H_2O column vectors out of S_m, defining a 'pruned' stoichiometric matrix, S'_m. The third term in this expression drops out if the activity of water is unity. Multiplying through by the inverse of S'_m, gives:

$$L'_{ab} + (S'_m)^{-1} S_{H+} \equiv L_{ar} = (S'_m)^{-1} L_K, \qquad (2)$$

where L_{ar} is a vector consisting of the log activity ratios of all the basis species. The dissolution reaction for carbon dioxide gas is: $CO_2(g) \rightarrow H^+ + HCO_3^- - H_2O$. We take the activity coefficient of H_2CO_3 (in solution) to be unity. We do not consider the impact of solution ionic strength on CO_2 (g) solubility (salting out effect). Pore fluid salinity is not important because P_{CO_2} depends on the bicarbonate activity ratio, which is fixed by the rock buffer independent of pH. The mass action equation for the CO_2 (g) dissolution reaction is thus:

$$\log a_{CO_2} = \log P_{CO_2} = \log a_{HCO_3^-} a_{H^+} - \log K_{CO_2(g)}, \qquad (3)$$

and we see that the log P_{CO_2} can be computed directly from the log of the bicarbonate activity ratio and the CO_2 dissolution log K.

Equation (4a–c) expresses eqn (2) in expanded form for the three buffers we consider here. In these equations the dissolution log K are evaluated at 200°C using the HKF equation of state and the SUPCRT thermodynamic database (see Johnson *et al.* 1992). In evaluating the log K for the calcite buffer (4a), we assume that the pore waters lie on the two-phase curve of water, as is appropriate in hydrothermal systems, so the pressure is 16 bars at 200°C. For the siderite and magnesite buffers we use the generalized basin pressure–temperature profile suggested by Smith & Ehrenberg (1989), and the pressure at 200°C is 1050 bars. The rows and columns of the stoichiometric matrix are labeled to indicate the buffer minerals and the basis species they represent. These annotations are, or course, not part of the equation. The stoichiometric matrix describes the dissolution of the buffer minerals to the basis species, so, for example, laumontite dissolves:

$$Ca[Al_2Si_4O_{12}]\cdot 4H_2O \rightarrow 2Al^{3+} + Ca^{2+} + 8H_2O - 8H^+ + 4SiO_2.$$

with the H^+ term incorporated in the activity ratio and the H_2O term dropped because the activity of water is unity, the result is the second row of the stoichiometric matrix in (4a).

$$\begin{bmatrix} \log a_{Al^{3+}}/a^3_{H^+} \\ \log a_{Ca^{2+}}/a^2_{H^+} \\ \log a_{HCO_3^-} a_{H^+} \\ \log a_{SiO2} \end{bmatrix} = \begin{bmatrix} & Al^{3+} & Ca^{2+} & HCO_3^- & SiO_2 \\ \text{calcite} & 0 & 1 & 1 & 0 \\ \text{laumontite} & 2 & 1 & 0 & 4 \\ \text{kaolinite} & 2 & 0 & 0 & 1 \\ \text{quartz} & 0 & 0 & 0 & 1 \end{bmatrix}^{-1} \begin{bmatrix} L_K \\ -0.61 \\ -1.12 \\ -4.87 \\ -2.44 \end{bmatrix} = \begin{bmatrix} 0.01 \\ 8.63 \\ -9.23 \\ -2.44 \end{bmatrix} \qquad (4a)$$

$$\begin{bmatrix} \log a_{Al^{3+}}/a_{H^+}^3 \\ \log a_{Fe^{2+}}/a_{H^+}^2 \\ \log a_{HCO_3^-} a_{H^+} \\ \log a_{SiO2} \end{bmatrix} = \begin{bmatrix} & Al^{3+} & Fe^{2+} & HCO_3^- & SiO_2 \\ \text{siderite} & 0 & 1 & 1 & 0 \\ \text{daphnite} & 2 & 5 & 0 & 3 \\ \text{kaolinite} & 2 & 0 & 0 & 2 \\ \text{quartz} & 0 & 0 & 0 & 1 \end{bmatrix}^{-1} \times \begin{bmatrix} L_K \\ -2.55 \\ 18.23 \\ -3.61 \\ -2.30 \end{bmatrix} = \begin{bmatrix} 0.50 \\ 4.83 \\ -7.37 \\ -2.30 \end{bmatrix} \quad (4b)$$

$$\begin{bmatrix} \log a_{Al^{3+}}/a_{H^+}^3 \\ \log a_{Mg^{2+}}/a_{H^+}^2 \\ \log a_{HCO_3^-} a_{H^+} \\ \log a_{SiO2} \end{bmatrix} = \begin{bmatrix} & Al^{3+} & Mg^{2+} & HCO_3^- & SiO_2 \\ \text{magnesite} & 0 & 1 & 1 & 0 \\ \text{daphnite} & 2 & 5 & 0 & 3 \\ \text{kaolinite} & 2 & 0 & 0 & 2 \\ \text{quartz} & 0 & 0 & 0 & 1 \end{bmatrix}^{-1} \times \begin{bmatrix} L_K \\ -0.77 \\ 28.34 \\ -3.61 \\ -2.30 \end{bmatrix} = \begin{bmatrix} 0.50 \\ 6.85 \\ -7.62 \\ -2.30 \end{bmatrix} \quad (4c)$$

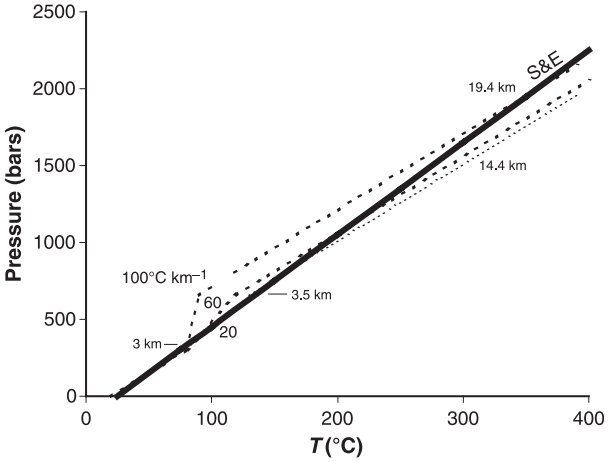

Fig. 2. The basin *P–T* trajectory proposed by Smith & Ehrenberg (1989) in which *P* (bars) = 6 (*T*(°C) − 25) compares well with 'more realistic' *P–T* trajectories which are shown by dashed lines. In the 'realistic' *P–T* trajectories, hydrostatic conditions and a geothermal gradient of 20°C km^{-1} (from a surface temperature of 20°C) pertain to 3 km depth, where a transition over 0.5 km takes pressure to lithostatic levels (660 bars at 220 bars km^{-1}). The pressure gradient is again hydrostatic below the seal. The thermal gradient in the half kilometer pressure transition varies from 20° to 100°C km^{-1} as indicated. The realistic *P–T* profiles are not significantly different than the Smith and Ehrenberg *P–T* trajectory. This shows the general appropriateness of the Smith and Ehrenberg *P–T* trajectory for P_{CO_2} calculations.

At 200°C and 16 bars $\log K_{CO_2}(g)$ equals −9.23. At 200°C and 1050 bars it equals −9.2. Combining the bicarbonate log activity ratios in the above expressions (third value in last column in 4a–c) with these $\log K_{CO_2}(g)$ values, as shown in eqn (3), gives $\log P_{CO_2} = -0.03$, 1.83, and 1.58 for the calcite, siderite, and magnesite buffers, respectively. These log partial pressures are plotted on Fig. 1 at 200°C. Partial pressures at other temperatures (and pressures) are calculated in a similar fashion and plotted to produce the buffer curves plotted on that figure. Again, in the calcite buffer case, pressure is chosen so that the water lies on the two-phase curve of water. In the siderate and magnesite buffer cases, the Smith and Ehrenberg pressure–temperature relationship shown in Fig. 2 is used [*P* (bars) = 6 (*T* (°C) − 25)]. Figure 2 shows that this is a reasonable *P–T* profile for basins that become overpressured at depth.

The curves calculated and plotted in Fig. 1 match the data shown in that figure quite well. The hydrothermal data are matched well by the hydrothermal buffer (4a), and the Smith and Ehrenberg non-anomalous basin CO_2 (S&E) data are matched will by the siderite and magnesite buffers (4b,c). The reason that the S&E CO_2 fugacities are higher than the hydrothermal CO_2 fugacities is that Ca-silicate minerals are absent in the S&E case. Fe or Mg silicate minerals are present instead. Because silicate calcium is not available, CO_2 cannot be precipitated as calcium carbonate, but only as iron carbonate (siderite) or magnesium carbonate (magnesite), and the fugacity of CO_2 along the S&E trend is higher than along the hydrothermal trend where calcium aluminosilicates are present.

Figure 3 plots the ratio of the sum of the partial pressures of the gas phases (steam plus CO_2) in equilibrium with the chemically buffered pore fluid, calculated as described above, to the total fluid pressure along the *P–T* profile [*P* (bars) = 6 (*T* (°C) − 25)] shown in Fig. 2. When this ratio equals unity, the gas pressure equals the total fluid pressure, and a separate gas phase can and will form. Figure 3 shows that this will occur at temperatures of approximately 330°C where iron or magnesium carbonates are present. $P_{CO_2}/P_{tot} = 1$ at 330°C for the siderite, and at 340°C for magnesite buffer. Coudrain-Ribstein *et al.* (1998) show that nearly as high partial pressures of CO_2 can be produced by a buffer that contains two carbonates (e.g. disordered dolomite and calcite), so the CO_2 source region need not necessarily contain magnesite or siderite. The essential conclusion at this point is that a separate CO_2-rich gas phase can be produced in sedimentary basins if the sediments reach temperatures of approximately 330°C.

CO_2 MIGRATION AND TITRATION

Because of its buoyancy, a CO_2-rich gas phase that is produced in a basin at approximately 330°C will have a strong tendency to migrate upward. If this occurs the migrating

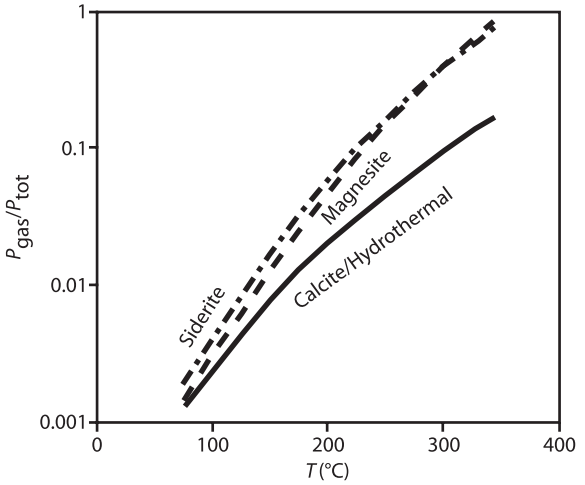

Fig. 3. Gas pressure (P_{CO_2} + P_{steam}) divided by pore fluid pressure (P_{tot}) calculated for the calcite, siderite and magnesite buffers as a function of temperature with pressure determined from the S&E *P–T* trajectory shown in Fig. 2. When the gas to total pressure ratio reaches 1, a separate CO_2-rich gas phase will exsolve from the pore fluids. High mole fraction CO_2 are produced where basin sediments with siderite or magnesite are heated to temperature approximately >330°C. The figure suggests that for calcite to break down temperatures of approximately 500°C would be required. However, interfingered/mixed calcite and dolomite may produce a CO_2-steam gas at temperatures less than this as discussed in the text.

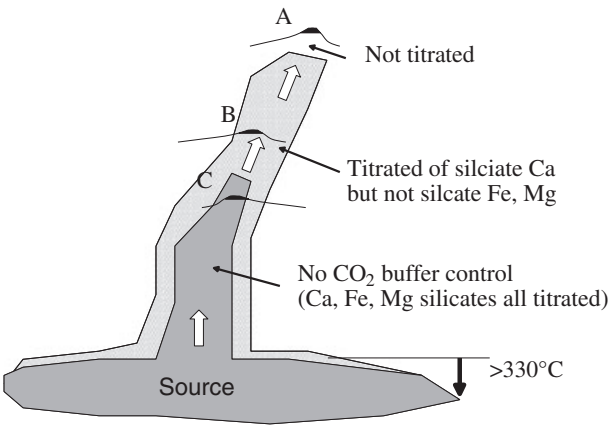

Fig. 4. Conceptual scheme of CO_2 generation and titration during migration. Carbonates are destroyed to produce CO_2 in sediments being heated to temperatures >330°C. The CO_2 migrates outward and upward where it is titrated first to the 'S&E magnesite or siderite' buffer levels and then to the very low 'calcite' buffer levels as first Fe- or Mg-silicates, and later Ca-silicates are encountered. Reservoirs filled at position A will have no CO_2. Reservoirs at position B will have moderate levels of CO_2 (as shown in Fig. 1). Reservoirs filled at position C could contain 100% CO_2 gas.

CO_2 gas will dissolve, and the concentration of total CO_2 in the pore fluids may rise above that which is in equilibrium with the sediment (buffer) minerals. Basin pore fluids are observed to be in local chemical equilibrium with their host sediments, and so, if this occurs, the CO_2-generating reaction must run in reverse: aluminosilicates must react and contribute Ca^{++}, Fe^{++}, or Mg^{++} to the solution. This will cause calcite, siderite, or magnesite to precipitate until the pore fluid is returned to chemical equilibrium with the sediment minerals.

Our combined migration and titration model can be summarized: As illustrated in Fig. 2, temperatures of approximately 330°C typically occur in the deep (>8 km) parts of active rift basins. They can occur at shallower depths if igneous sills or plutons intrude the basin sediments. As illustrated in Fig. 4, CO_2 is generated at the rate that this part of the basin is heated above 330°C (by burial or by an intrusion). In this zone carbonates are destroyed, Ca-, Fe-, and Mg-aluminosilicate clay minerals produced, and CO_2 generated. As the high mole fraction CO_2 gases generated deep in a basin migrate upward and outward it may be joined by CH_4. As the gases migrate to cooler environments, the water in contact with them gets supersaturated with respect to carbonate minerals because of the high P_{CO_2} in the migrating gas stream. Initially, calcium carbonate will be most supersaturated, and calcium aluminosilicates will be destroyed to obtain the Ca needed to restore chemical equilibrium between the fluid and rock. As long as Ca-aluminosilicate minerals are present the partial pressure of CO_2 in any gas phase will be buffered to very low levels and the appropriate carbon dioxide buffer level will be that of the calcite buffer in Fig. 1. When Ca-silicate phases are exhausted and Ca is no longer available, the CO_2 will react with Fe- and Mg-aliminosilicates to form siderite and magnesite. The buffer levels of the migrating gas will rise to the siderite and magnesite (S&E) buffers in Fig. 1 so long as Fe- or Mg-silicates are available. When Fe- and Mg-silicates are exhausted, the CO_2 concentrations will be unbuffered, and gases will move through the sediments with no loss of CO_2 partial pressure.

The zones of reaction will move upward and outward from the source as shown in Fig. 4. Near the source and along the pathways through which a great deal of CO_2 has passed, the Ca-, Fe-, and Mg-aluminosilicates will all have reacted out, and the mole fraction of CO_2 in the gas phase can be very high. Further out, where Ca-aluminosilicates are gone but Fe- and Mg-aluminosilicates still remain, the mole fraction of CO_2 in the migrating gas will be reduced to lower, but still appreciable, levels. Still further from the source, where Ca-aluminosilicates are present, the mole fraction of CO_2 in the migrating gas will be buffered to negligible levels, and CO_2 will not be a significant component in the gas that fills any reservoirs.

The CO_2 titration and carbonate precipitation cannot occur in the reservoir, but must rather occur along the migration pathways, which may be a single broad pathway as illustrated in Fig. 4, or multiple, narrow fingers of migration along faults or the most permeable parts of strata, depending on the local geology. The reason that

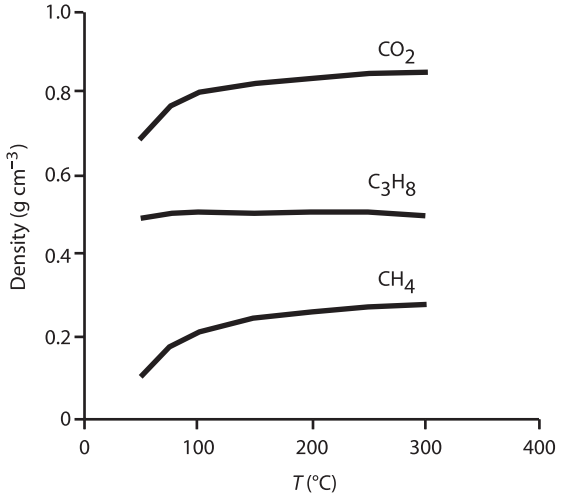

Fig. 5. The density of selected gases along the S&E basin *P–T* trajectory calculated with the (Behar & Simonet 1985) equation of state.

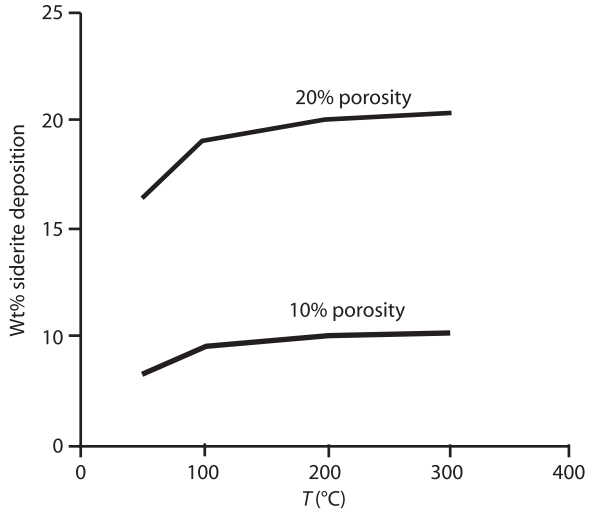

Fig. 6. The siderite precipitation required to reduce a high mole fraction gas charge to the S&E buffer limits for sediments with 10% and 20% porosity.

the CO_2 titration and carbonate precipitation must occur along the migration pathways is that if titration were to occur entirely in the reservoir, more intense carbonate precipitation would be required than is observed. Figure 5 shows the density of several gas phases computed along the S&E basin *P–T* trajectory. At basin pressures and temperatures, CO_2 is a remarkably dense gas phase. A high mole fraction CO_2 gas will have a density close to 0.8 g cm^{-3} when introduced to reservoirs at 100 and 200°C and pressures given by P (bars) = 6 (T (°C) − 25). The amount of siderite that must be precipitated to reduce one pore volume charge of CO_2 to S&E buffer levels is shown in Fig. 6. This figure shows that the weight percent siderite precipitated is approximately equal to the porosity of the sediment. A sediment with 20% porosity must precipitate about 20 wt% siderite to reduce the CO_2 mole fraction of a nearly pure CO_2 gas charge to S&E buffer levels; a 10% porosity sediment must precipitate about 10 wt% siderite. Carbonate precipitation this intense is not generally observed in reservoirs, and we take this as evidence that the titration of CO_2 from >330°C kitchens occurs along the gas migration path, not locally within gas-charged reservoirs. Siderite and magnesite precipitation can be less intense if distributed along the migration pathways, but might still be marked enough to be observed in drill core and perhaps by geophysical methods.

INCORPORATION OF THE CO_2 SOURCE-TITRATION MODEL INTO A BASIN MODEL

The conceptual model of CO_2 generation and titration along migration pathways as shown in Fig. 4 can be incorported into a conventional basin model and the processes we have described thereby quantitatively simulated. The basin model we use is a conventional one of our own design. Sediments are added in layers, and the compaction of underlying sediments due to the increase in effective stress induced by this added load computed. Pore pressure is increased by the load and relaxed over the timestep as allowed by sediment and fault permeability. Temperature is calculated for geologically reasonable, porosity- and temperature-dependent sediment thermal conductivities subject to the proscribed heat flow into the base of the basin. Pore fluids moving from compacting layers or where expelled by positive-volume hydrocarbon maturation reactions, follow paths dictated by the porosity-dependent strata permeability and the assigned fault permeabilities. The model is described in Cathles & Losh (2002) and also in a user's manual (Cathles 2003) that is available on the worldwide web.

CO_2 generation and reaction are added to this conventional basin model in the following way: Carbonate in a finite element is assumed to convert to CO_2 as that element is heated above 320°C. This CO_2 then moves parallel to the flow of basin fluids, but cannot pass through a cooler element until enough CO_2 has entered the element to fully satisfy its CO_2 titration capacity. CO_2 is deposited in these elements as carbonate, and this carbonate can react to produce CO_2 if the element is subsequently heated above 320°C. The model does not distinguish the titration of calcium aluminosilicates from Mg and Fe aluminosilicates. It simply identifies paths that are fully titrated of all CO_2-buffering capacity. Along these pathways reservoirs could be filled with 100% CO_2 gas.

Numerical modeling requires estimates of the CO_2 generation and titration capacity of the sediments. These numbers vary from basin to basin and should be specifically

Table 1 Typical shale chemistries from Potter *et al.* (1980).

Component	wt%	moles cm^{-3} sediment
CaO	3.11	5.55×10^{-4}
MgO	2.44	3.03×10^{-4}
FeO	2.45	1.71×10^{-4}
CO2	2.65	1.5×10^{-4}

estimated for the particular basin being modeled. In the absence of specific data, the values for a typical shale that are given in Table 1 can be used. We use these values in the calculation presented in this paper.

From Table 1 it can be seen that the total titratable silicate cation content of an average shale is 8.8×10^{-4} moles cm^{-3} of sediment (the total reduced oxide cation content minus the moles tied up in carbonates), and the CO_2-generating capacity of a typical shale is 1.5×10^{-4} moles CO_2 cm^{-3} of shale. We assume that all the CO_2 can be produced from the sediment, but that about half the overlying sediments would be bypassed and thus the overlying sediments will be only about half titrated of CO_2-neutralizing silicate cations. The CO_2 titration capacity of typical shale is therefore taken to be 4.4×10^{-4} moles CO_2 cm^{-3} of sediment.

The output of our finite element basin model simulations is (i) the location of the CO_2 source regions in a basin and, (ii) the location of sediments that have been titrated of their silicate Ca, Fe and Mg content by interaction with CO_2. These titrated zones, and their reasonable geologic extensions, are the areas where the risk is highest of encountering reservoirs with high mole fractions of CO_2.

MODELING RESULTS AND AN APPLICATION TO THE SOUTH CHINA SEA

Figures 7 and 8 show the results of incorporating CO_2 generation and titration in a basin model. Figure 7 shows, in a very simple situation, how CO_2 generated deep in a basin can move up permeable structures, and titrate all the aluminosilicates within them that could buffer CO_2 fugacity. Nowadays, the risk of encountering CO_2 in gas reservoirs over the two fully titrated vertical structures would be very high.

Figure 8 shows a simulation of CO_2 generation and migration in a cross section whose geology is known from seismic and drill hole data. The section runs to the northeast from an area of mud volcanoes in the center of the Yinggehai basin in the South China Sea. The CO_2 generated in the very deep central parts of this basin has, according to the model simulation, titrated a large volume of sediments of the aluminosilicates that could buffer CO_2 to low levels. The risk of reservoirs having high CO_2 over the deepest part of the basin near the mud volcanoes is great, but the risk in areas nearer the margin to the east and north is low, according to our generation-titration model. These predictions are in accord with documented CO_2 in reservoirs drilled in the area to date (see Huang *et al.* 2005).

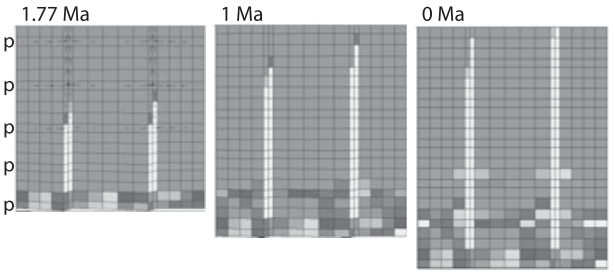

Fig. 7. Simulation of CO_2 titration in a basin with two permeable vertical channels (white columns) and four permeable strata (arrows and 'p' annotation on 1.77-Ma section). Sediments are deposited and the section grows in thickness with time. Age is indicated at the top of each section, and strata are indicated by black horizontal lines. The arrows indicate water flow. Their upward increase in size indicates the dominance of compaction in driving pore fluid flow. CO_2 is generated where the growing section moves across the 320°C isotherm (roughly the elevation of the top of the colored (mottled in black and white) band in the 1.77 Ma section). CO_2 generated in this source zone is focused by the permeable strata (labeled 'p') into the vertical channels, and the channels quickly become titrated of their CO_2-buffering capacity, as indicated by their white color. Colors show where the CO2 titration capacity (initially green and ending in white) has been reduced by reaction with CO_2. Reservoirs at the tops of the vertical channels at the present day ($t = 0$ Ma section) would have a high probability being filled with gas with a high mole fraction of CO_2.

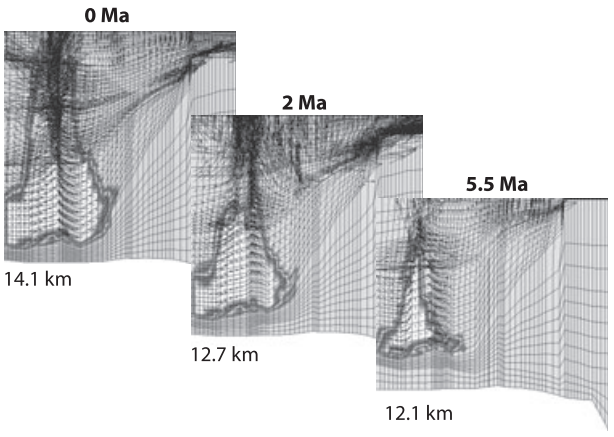

Fig. 8. A 101 km NE–SW section running SW to NE from the middle of the Yinggehai Basin showing the development of the zone where Ca-, Fe-, and Mg-aluminosilicates have been titrated by reaction with CO_2 generated in the deeper parts of the basin. Sections are shown at 0, 2, and 5.5 Ma before present. The section at 0 Ma is based on stratigraphy inferred from seismic surveys. The other sections are obtained from the first by backstripping and decompacting as described in the text. The numbers in the lower left give the thickness of this part of each section.

SUMMARY AND DISCUSSION

In this paper we have described a conceptual model for CO_2 generation and titration in basins which, when quantified and incorporated into a conventional basin model, makes CO_2 risk predictions that are compatible with exploration experience in at least some areas. The conceptual model explains why most gas reservoirs contain negligible amounts of CO_2, while some gas reservoirs contain a few weight percent CO_2 which increases logarithmically with reservoir temperature along what we call the S&E trend. Moreover, our model explains why some reservoirs contain gas that is almost 100% CO_2, and why the reservoirs with moderate to high CO_2 are associated with particularly thick sediment accumulations. In the model, CO_2 is generated where carbonates in basin sediments are heated to temperatures >330°C. Where this occurs, the partial pressures of CO_2 and steam are equal to the local pore fluid pressures, and a separate CO_2-rich gas phase forms which can migrate upward into cooler sediments where the CO_2 reacts with Ca-, Fe-, and Mg-aluminosilicates to form carbonates again. When the Ca-aluminosilicates are destroyed by reaction, the levels of CO_2 in the gas are moderate, depend on temperature, and lie along the S&E buffer trend in Fig. 1. When the Fe- and Mg-aluminosilicates are destroyed by reaction with the CO_2 gas, all buffer control on CO_2 concentration is removed, and reservoirs can be filled with gas that is 100% CO_2. We describe how these concepts can be incorporated into a conventional basin model, and illustrate the results that can be obtained when this is done.

The conceptual and numerical models make a number of assumptions that warrant discussion. First the nature of CO_2 buffers bears some comment. Coudrain-Ribstein *et al.* (1998) recently analyzed a set of six mineral buffers that can match the S&E trend in Fig. 1. In general the buffers they identify lack a Ca-silicate phase, as we suggest should always be the case. One of their buffers (disordered dolomite-calcite-chlorite-zoisite-quartz) shows high fugacities of CO_2 despite the presence of a Ca-aluminosilicate. However, for this buffer, margarite is supersaturated by nearly 3 orders of magnitude at 200°C. If margarite is substituted for their buffer mineral zoisite, kaolinite is supersaturated by an order of magnitude. Substituting kaolinite yields a buffer of disordered dolomite-calcite-kaolinite-chlorite-quartz which sustains a high P_{CO_2} but does not contain a Ca-aluminosilicate, and hence does not violate our rules. Valid buffers should not contain supersaturated minerals. Once a CO_2-rich gas phase leaves its source, its fate will depend on the availability of Ca-, Fe- and Mg-silicates as we have described. We do not seek here to tailor a set of buffer minerals and their stoichiometry to that appropriate for a particular locality and show that such a mineral set exists there. This should be done, but it is beyond the scope of the present paper. Our purpose here is only to articulate the concept of a source-titration model in general terms and show how it can be quantified.

Apart from the nature and operation of the mineral buffers, the most critical assumption we make is probably that basement rocks will not be a source of CO_2. The main argument for this assumption is that, as all basins cause rock at some depth into basement to move through the 330°C isotherm, if CO_2 could be generated in basement rocks then all basins should have roughly equal CO_2 risk, and this does not seem to be the case. Rather, risk seems to be concentrated in active basins with thick sediment accumulations. There are some good reasons why the basement may not typically be a good source for CO_2. The titration capacity of basement rocks is likely to be large because they are commonly less weathered than basin shales and therefore should have higher concentrations of Ca-, Fe-, and Mg-silicate minerals. At great depth, the density of CO_2 might be greater than water, and CO_2 might not be able to escape as easily or at all. Low basement permeability may inhibit the outgasing of CO_2, and the CO_2 that does escape may be channeled to major basement faults, and thus pose less of a distributed risk to hydrocarbon exploration. Deeper basement rocks may typically have been previously heated above 330°C and their CO_2-generating capacity expended. Nevertheless these arguments may not be valid in all cases and the possibility that CO_2 might be generated in basement rocks below basin sediments should not be neglected.

We have also ignored biogenic CO_2 generation, and the thermogenic generation of CO_2 from organic material. Organic CO_2 generation could be substantial in some cases, and its titration would reduce the CO_2 titration capacity of the sediments when CO_2 is later generated inorganically. Seewald *et al.* (1998) and Seewald (2003) provide discussion that is also of interest because it involves inorganic mineral buffering. Moreover, CO_2 is commonly vented from igneous intrusions (e.g. Ballentine *et al.* 2001). In areas with magmatic activity, this kind of CO_2 supply should be remembered.

Finally the models we describe do not couple methane generation to CO_2 migration and titration. Methane generation could affect the flow paths of the gas by decreasing its density and promoting buoyant vertical flow. Additions of methane after a reservoir fills with CO_2 could erase much of the CO_2 risk we predict.

Despite all the assumptions and approximations made, the present model appears to make useful predictions of CO_2 risk. Where applied to date it has produced results consistent with known CO_2 exploration risk with no 'tuning'. This can be appreciated by comparing Fig. 8 to the L8-1 profile in Huang *et al.* (2005). The insights provided by the model, and the experience we have gained from basins that we have analyzed to date, suggest that a few

critical parameters can provide an estimate of the CO_2 risk at the location of a particular well. The critical parameters include the ratio of CO_2 generation to total potential titration at the basin center and at the margin nearest the well, and the proximity of structures to the well. The numerical modeling described above thus provides a basis for much simpler methods of data evaluation and risk management.

The model presented also has interesting and perhaps important scientific implications. The migration routes of natural gases in basins are of both practical and scientific interest. Practically, knowing the migration pathways might usefully direct exploration to areas where traps would be less likely to be filled with CO_2. Scientifically, we would like to know how fluids of various kinds move through faulted sediments. This has proven remarkably difficult, and there is broad disagreement about even such fundamental issues as whether hydrocarbons move in faults at all, or only in the fractured zones adjacent to faults. Examining the alteration pattern produced by the passage of a reactive gas such as CO_2 could provide a way to answer some of these questions, particularly since the source of CO_2 can be highly localized, as it is when the CO_2 emanates from or is generated by the heat from an intrusion.

ACKNOWLEDGEMENTS

The work on which this paper is based was carried out by the authors while the first author was at Cornell and the second author at Chevron. A 1996 report to Chevron prepared by the first author forms the basis for much of the text. We are thankful to Chevron for past support, and for permission to publish the results of the work they funded. We would like to acknowledge the assistance of members of the CO_2 Chevron study team, including especially Alex Erendi, Steve Patti, and Noelle Schoellkopf, and the help of Barry Katz in securing the proper permissions to publish. We are also grateful for the helpful suggestions of two reviewers, one anonymous. We thank particularly Kurt Bucher and *Geofluids* editor Bruce Yardly for encouraging a more detailed presentation of the modeling methods.

REFERENCES

Arnorsson S, Gunnlaugsson E, Svavarsson H (1983) The chemistry of geothermal waters in Iceland. II. Mineral equilibria and independent variables controlling water compositions. *Geochimica Cosmochimica Acta*, **47**, 547–66.

Ballentine C, Schoell M, Coleman D, Cains BA (2001) 300-Myr-old magmatic CO2 in natural gas reservoirs of the west Texas Permian basin. *Nature*, **409**, 327–31.

Baylis P, Levinson AA (1971) Low temperature hydrothermal synthesis for dolomite or calcite, quartz and kaolinite. *Clay and Clay Minerals*, **19**, 109–14.

Behar E, Simonet R (1985) A new non-cubic equation of state. *Fluid Phase Equilibria*, **21**, 237–55.

Boon JA, Hitcheon B (1983) Application of fluid-rock reactions studies to in situ recovery from oil sand deposits, Alberta, Canada-II. Mineral transformations during experimental-statistical study of water-bitumen-shale reactions. *Geochimica Cosmochimica Acta*, **47**, 249–57.

Cathles LM (1986) The geologic solubility of gold from 200–350°C, and its implications for gold-base metal ratios in vein and stratiform deposits. *Canadian Institute of Mining and Metallurgy*, **38** (Special Volume), 187–210.

Cathles LM (1993) Oxygen isotope alteration in the Noranda Mining District, Abitibi greenstone belt, Quebec, Canada. *Economic Geology*, **88**, 1483–512.

Cathles LM (2003) *Processing Geologic Cross Sections to Estimate Hydrocarbon Production, Migration and Chemistry*, User's manual for BasinLAB software, http://www.geo.cornell.edu/geology/easresearch/geomodeling/basinlab/AgeohistFinalReport4.pdf, 167 p.

Cathles LM, Losh SL (2002) A modeling analysis of the hydrocarbon chemistry and gas washing, hydrocarbon fluxes, and reservoir filling, vol. IV. In: *Seal Control of Hydrocarbon Migration and its Physical and Chemical Consequences* (ed. Cathles LM), 63 p. Gas Research Institute, Des Plaines, Report GRI-03/0065.

Cathles LM, Schoell M, Simon R (1990) A kinetic model of CO2 generation and mineral and isotopic alteration during steamflooding. *SPE Reservoir Engineering*, November, 524–30.

Coudrain-Ribstein A, Gouze P, de Marsily G (1998) Temperature-carbon dioxide partial pressure trends in confined aquifers. *Chemical Geology*, **145**, 73–89.

Elder J (1981) *Geothermal Systems*. Academic Press, London, 508 p.

Ellis AJ (1970) Quantitative interpretation of chemical characteristics of hydrothermal systems. *Geothermics*, **2**, 516–28.

Giggenbach WF (1981) Geothermal mineral equilibria. *Geochimica Cosmochimica Acta*, **45**, 393–410.

Giggenbach WF (1997) Relative importance of thermodynamic and kinetic processes in governing the chemical and isotopic composition of carbon gases in high-heatflow sedimentary basins. *Geochimica Cosmochimica Acta*, **61**, 3763–85.

Hanor JS (1994) Physical and chemical controls on the composition of waters in sedimentary basins. *Marine and Petroleum Geology*, **11**, 31–45.

Hanor JS (2001) Reactive transport involving rock-buffered fluids of varying salinity. *Geochimica Cosmochimica Acta*, **65**, 3721–32.

Hebner BA, Bird GW, Lngstaff FJ (1986) Fluid-pore mineral transformations during steam injection: implications for reduced permeability damage. *Journal of Canadian Petroleum Technology*, Sept–Oct, 68–73.

Henley RW, Truesdell AH, Barton PB (1984) Fluid-mineral equilibria in hydrothermal systems. *Reviews in Economic Geology*, **1**, Society of Economic Geologists, El Paso, 267 p.

Huang B, Xiao A, Hu Z, Yi P (2005) Geochemistry and episodic accumulation of natural gases from the Ledong gas field in the Yinggehai Basin, offshore South China Sea. *Organic Geochemistry*, **36**, 1689–702.

Hutcheon I, Shevalier M, Abercrombie HJ (1993) pH buffering by metastable mineral-fuid equilibria and evolution of carbon dioxide fugacity during burial diagenesis. *Geochimica Cosmochimica Acta*, **57**, 1017–27.

Johnson JW, Oelkers EH, Helgeson HC (1992) SUPCRT92: A software package for calculating standard molar thermodynamic properties of mineras, gases, aqueous species, and reactions from 1 to 5000 bars and 0 to 1000°C. *Computers in Geoscience*, **18**, 899–947.

Kubacki W, Boon J, Bird G, Wiwchar B (1984) Effect of mineral transformation on porosity and permeability of dolomite rock during in situ recovery of bitumen: a preliminary study. *Bulletin of Canadian Petroleum Geology*, **32**, 281–8.

Leong KM (Ed.) (2000) *The Petroleum Geology and Resources of Malaysia*, Petronas (Petroliam Nasional Berhad), Kuala Lumpur, 665 p. ISBN 983-9738-10-0.

Levinson AA, Vian RW (1966) The hydrothermal synthesis of montmorillonite group minerals from kaolinite, quartz, and various carbonates. *American Mineralogist*, **31**, 495–8.

Muffler PJ, White DE (1968) Origin of CO_2 in the Satton Sea Geothermal System, Southeastern California, USA. *XXIII International Geological Congress*, **17**, 185–94.

Palandri JL, Reed MH (2001) Reconstruction of in situ composition of sedimentary formation waters. *Geochimica Cosmochimica Acta*, **65**, 1741–67.

Potter PE, Maynard JB, Pryor WA (1980) *Sedimentology of Shale*. Springer-Verlag, New York, 306 p.

Seewald JS, Benitez-Nelson BC, Whelan JK (1998) Laboratory and theoretical constraints on the generation and composition of natural gas. *Geochimica Cosmochimica Acta*, **62**, 1599–617.

Seewald JS (2003) Organic–inorganic interactions in petroleum-producing sedimentary basins. *Nature*, **426**, 327–33.

Smith JT, Ehrenberg SN (1989) Correlation of carbon dioxide abundance with temperature in clastic hydrothermal reservoirs: relationship to inorganic chemical equilibrium. *Marine and Petroleum Geology*, **6**, 129–35.

Wilson GA (1994) Mineral-fuid equilibria in deeply buried sandstones at McAllen Ranch Field, S. Texas. Geological Society of America Abstracts with Programs, A-279.

Wycherley H, Fleet A, Shaw H (1999) Some observations on the origins of large volumes of carbon dioxide accumulations in sedimentary basins. *Marine and Petroleum Geology*, **16**, 489–94.